Control of ciliogenesis by FOR20, a novel centrosome and pericentriolar satellite protein

Fatima Sedjaï[1,2,3,*], Claire Acquaviva[1,2,3,*], Véronique Chevrier[1,2,3], Jean-Paul Chauvin[3,4], Emilie Coppin[1,2,3], Aicha Aouane[3,4], François Coulier[1,2,3], Aslihan Tolun[5], Michel Pierres[3,6], Daniel Birnbaum[1,2,3] and Olivier Rosnet[1,2,3,‡]

[1]Centre de Recherche en Cancérologie de Marseille, UMR 891 INSERM, F-13009 Marseille, France
[2]Institut Paoli-Calmettes, F-13009 Marseille, France
[3]Université de la Méditerranée, F-13007 Marseille, France
[4]Institut de Biologie du Développement de Marseille-Luminy, UMR 6216 CNRS, F-13009 Marseille, France
[5]Department of Molecular Biology and Genetics, Boğaziçi University, Istanbul 34342, Turkey
[6]Centre d'Immunologie de Marseille-Luminy, UMR 6102 INSERM/CNRS, F-13009 Marseille, France

*These authors contributed equally to this work
‡Author for correspondence (olivier.rosnet@inserm.fr)

Accepted 21 April 2010
Journal of Cell Science 123, 2391-2401

doi:10.1242/jcs.065045

Summary

Cilia and flagella are evolutionary conserved organelles that generate fluid movement and locomotion, and play roles in chemosensation, mechanosensation and intracellular signalling. In complex organisms, cilia are highly diversified, which allows them to perform various functions; however, they retain a 9+0 or 9+2 microtubules structure connected to a basal body. Here, we describe FOR20 (FOP-related protein of 20 kDa), a previously uncharacterized and highly conserved protein that is required for normal formation of a primary cilium. FOR20 is found in PCM1-enriched pericentriolar satellites and centrosomes. FOR20 contains a Lis1-homology domain that promotes self-interaction and is required for its satellite localization. Inhibition of FOR20 expression in RPE1 cells decreases the percentage of ciliated cells and the length of the cilium on ciliated cells. It also modifies satellite distribution, as judged by PCM1 staining, and displaces PCM1 from a detergent-insoluble to a detergent-soluble fraction. The subcellular distribution of satellites is dependent on both microtubule integrity and molecular motor activities. Our results suggest that FOR20 could be involved in regulating the interaction of PCM1 satellites with microtubules and motors. The role of FOR20 in primary cilium formation could therefore be linked to its function in regulating pericentriolar satellites. A role for FOR20 at the basal body itself is also discussed.

Key words: Primary cilium, Pericentriolar satellites, Microtubule, Centrosome, PCM1

Introduction

Microtubule-based cilia and flagella are specialized cellular structures that appeared very early in eukaryote evolution. In present-day unicellular and multicellular organisms, cilia are involved in various biological processes such as force-generation, mechanosensation, chemosensation and regulation of signal transduction (Marshall and Nonaka, 2006; Satir and Christensen, 2007; Singla and Reiter, 2006). In vertebrates, specialized epithelial cells lining the airways, the oviduct and the brain ventricles, harbour multiple motile cilia to generate fluid flow. Every cilium extends from a modified centriole, the basal body, which docks at the membrane and provides a template for axoneme elongation (Marshall, 2008). The axonemal central core of motile cilia is made of nine microtubule doublets and one central microtubule pair, i.e. the 9+2 configuration. Motility requires the motor activities of inner and/or outer dynein arms to cause the doublet microtubules to slide with respect to one another. In vertebrates, a single non-motile cilium, referred to as a primary cilium, is found on many non-hematopoietic cells (Wheatley et al., 1996). The primary cilium lacks the central pair of microtubules and has the so-called 9+0 configuration. Non-motile cilia concentrate receptors and signalling machinery, such as effectors of phototransduction and olfaction, and molecular components of the WNT, Hedgehog and platelet-derived growth factor receptor α signalling pathways (Christensen et al., 2008; Gerdes and Katsanis, 2008; Wong and Reiter, 2008). This primary cilium serves as an antenna at the surface of cells.

Cilia formation is a multistep process that requires the docking of the basal body to the cell cortex, elongation of the cilium membrane and axoneme, and the specific recruitment of signalling molecules (Park et al., 2008; Pazour and Bloodgood, 2008). Little is known about the signal(s) that initiate the transformation of the mother centriole of the centrosome into a basal body. This transformation induces some changes in its structural characteristics and in the protein composition of the surrounding matrix (Dawe et al., 2007). The basal body not only docks at the membrane to allow cilium growth at the cell surface, it also participates in protein sorting at the transition fibres that connect the basal body to the cell membrane (Deane et al., 2001; Pedersen and Rosenbaum, 2008). This is an important aspect of cilium formation, as the composition of the cilium and its membrane are distinct from that of the cell body, and no protein synthesis occurs in this organelle. Once initiated, cilium elongation involves complex mechanisms that control growth of microtubules, localized membrane extension and sorting of various proteins into the cilium. Ciliogenesis strongly depends on intraflagellar transport (IFT). This transport is ensured by two multisubunit complexes called IFT particles A and B. These are associated with both kinesin 2 and cytoplasmic dynein 1b motors in order to promote bidirectional movements. IFT particles provide binding

Journal of Cell Science

sites for cilia components that need to be transported to the cilium but also need to be removed or recycled from the cilium. Tight regulation of IFT is thus proposed to control cilium size (Marshall et al., 2005; Marshall and Rosenbaum, 2001). In *C. elegans*, Bardet-Biedl syndrome (BBS) proteins promote IFT complexes cohesion and coordination (Blacque et al., 2004; Ou et al., 2005). BBS is a genetically heterogeneous syndrome linked to primary cilium deficiency. Individuals with BBS suffer from various defects, including obesity, retinal degeneration, mental retardation and renal cystic disease (Badano et al., 2006). A complex of seven out of the 12 known BBS gene products is important for cilium formation in vertebrate cells (Loktev et al., 2008; Nachury et al., 2007). This complex, called the BBSome, functions in part by regulating membrane extension through activation of RAB8, one of several small GTPases that are implicated in vesicular trafficking for cilia formation and function. The activity of the BBSome is also linked to acetylation of axonemal microtubules (Loktev et al., 2008). The BBSome is physically linked to PCM1-enriched pericentriolar satellites. The latter are 70-100 nm electron-dense granular structures that are involved in microtubule and dynein/dynactin-dependent recruitment of proteins to the centrosome (Dammermann and Merdes, 2002; Kubo et al., 1999; Kubo and Tsukita, 2003). Pericentriolar satellites may thus serve as vehicles to transport cargos to the centrosomes and basal bodies.

Despite mounting evidence about the importance of cilia in organism physiology and pathology, we still do not have a clear picture of how a cilium is built and what protein complexes perform each step of the ciliogenesis process. Here, we describe the identification and characterization of a novel highly conserved centrosome and pericentriolar satellite protein involved in primary cilium formation.

Results

Identification of a FOP-related protein in ciliated species

We used the tBLASTn program to find proteins with sequence similarity to the centrosomal FOP (FGFR1 Oncogene Partner) protein (Acquaviva et al., 2009; Popovici et al., 1999) and identified a small conserved putative protein showing low but significant similarity with FOP N-terminal region in humans. This putative new protein, C16orf63/FLJ31153 in GenBank, was named FOR20 (FOP-related protein of 20 kDa) (Fig. 1A,B). Remarkably, despite a low percentage of identity, a Lis1 homology (LisH) domain was predicted at a similar position in both FOP and FOR20. LisH

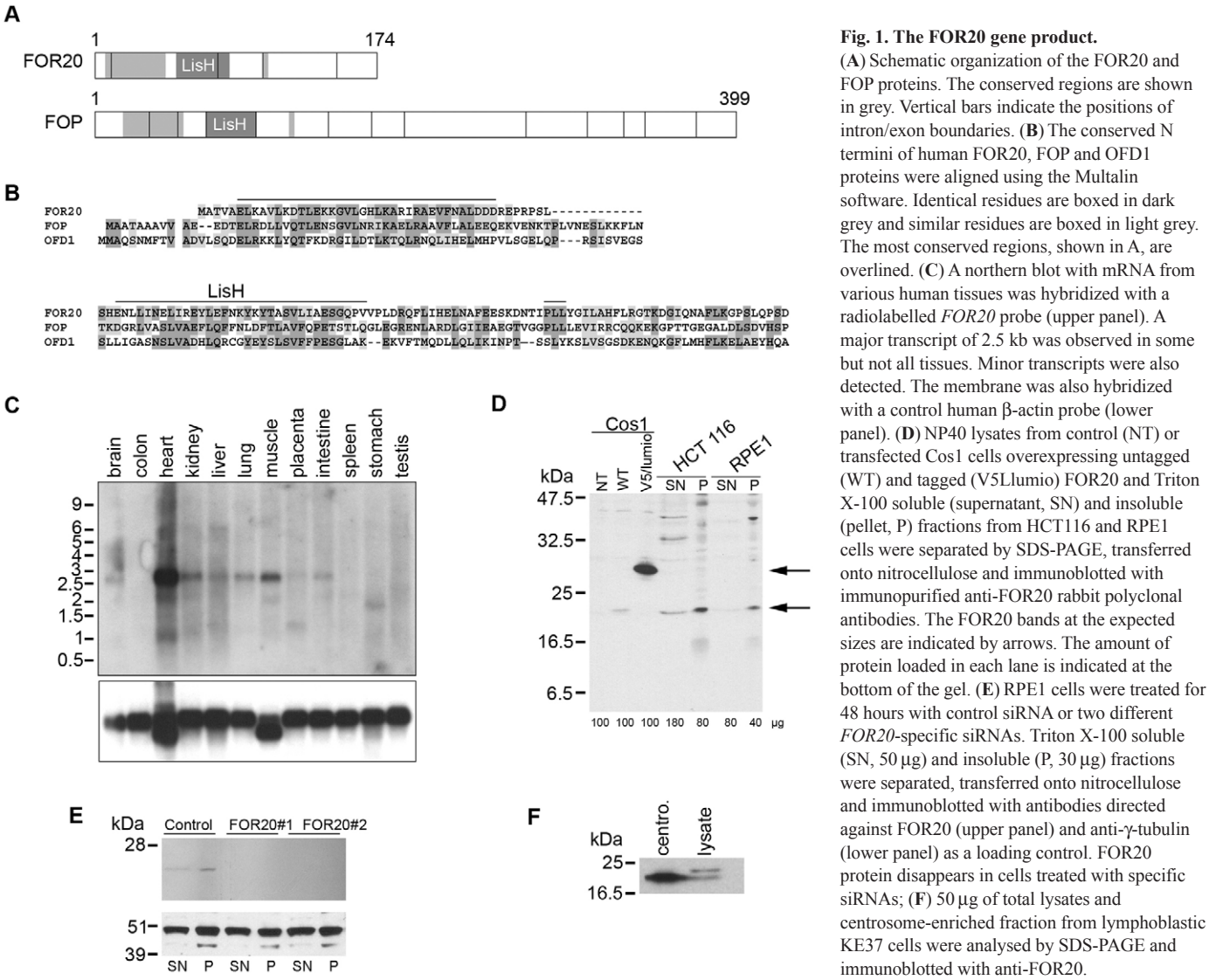

Fig. 1. The FOR20 gene product.
(**A**) Schematic organization of the FOR20 and FOP proteins. The conserved regions are shown in grey. Vertical bars indicate the positions of intron/exon boundaries. (**B**) The conserved N termini of human FOR20, FOP and OFD1 proteins were aligned using the Multalin software. Identical residues are boxed in dark grey and similar residues are boxed in light grey. The most conserved regions, shown in A, are overlined. (**C**) A northern blot with mRNA from various human tissues was hybridized with a radiolabelled *FOR20* probe (upper panel). A major transcript of 2.5 kb was observed in some but not all tissues. Minor transcripts were also detected. The membrane was also hybridized with a control human β-actin probe (lower panel). (**D**) NP40 lysates from control (NT) or transfected Cos1 cells overexpressing untagged (WT) and tagged (V5Llumio) FOR20 and Triton X-100 soluble (supernatant, SN) and insoluble (pellet, P) fractions from HCT116 and RPE1 cells were separated by SDS-PAGE, transferred onto nitrocellulose and immunoblotted with immunopurified anti-FOR20 rabbit polyclonal antibodies. The FOR20 bands at the expected sizes are indicated by arrows. The amount of protein loaded in each lane is indicated at the bottom of the gel. (**E**) RPE1 cells were treated for 48 hours with control siRNA or two different *FOR20*-specific siRNAs. Triton X-100 soluble (SN, 50 µg) and insoluble (P, 30 µg) fractions were separated, transferred onto nitrocellulose and immunoblotted with antibodies directed against FOR20 (upper panel) and anti-γ-tubulin (lower panel) as a loading control. FOR20 protein disappears in cells treated with specific siRNAs; (**F**) 50 µg of total lysates and centrosome-enriched fraction from lymphoblastic KE37 cells were analysed by SDS-PAGE and immunoblotted with anti-FOR20.

domains are involved in homodimer formation of various proteins (Gerlitz et al., 2005; Kim et al., 2004b; Mikolajka et al., 2006). The FOP and FOR20 proteins are also distantly related to the N terminus of the centrosomal OFD1 (oral facial digital 1) protein (Fig. 1B). A conserved PLL tripeptide was found close to the C terminus of the LisH domain in FOP and FOR20, but not in OFD1.

Subsequently, we extensively searched databases to identify gene products related to FOP and FOR20 in different species (supplementary material Fig. S1 and Table S1) and carried out a phylogenetic analysis. We defined two evolutionary clades that correspond to FOP and FOR20 orthologous proteins (supplementary material Fig. S2). A number of species in several taxons, i.e. alveolates, cnidaria, deuterosomia, ecdysosoa (arthropods) and lophotrocozoa (molluscs), have FOP and FOR20 orthologues, strongly suggesting that the corresponding genes are derived from a common precursor that duplicated early in the course of eukaryote evolution. Among these orthologues, the land plant FOP orthologue TON1 is the only protein characterized to date. TON1 is required for cortical microtubules and preprophase band formation (Azimzadeh et al., 2008). In contrast to FOP, FOR20 orthologues are only found in ciliated organisms, an indication that this protein could be involved in cilia function or formation.

Characterization of FOR20 expression

To determine in which tissues human *FOR20* was expressed, we hybridized a northern blot of polyadenylated RNAs with a *FOR20* cDNA probe (Fig. 1C). A major transcript of ~2.5 kb was observed in many tissues, i.e. brain, heart, kidney, liver, lung, skeletal muscle, placenta and intestine. The size of this transcript is close to the size of the full-length *C16orf63* mRNA (2250 bp; Accession Number, NM_144600), encoded by five exons on chromosome 16p13.11. Minor transcripts, mainly shorter, were also detected, which may correspond to variants predicted by EST analysis (http://genome.ewha.ac.kr/cgi-bin/ECquery.cgi?organism=human&query=C16orf63). RT-PCR experiments also showed *FOR20* expression in HeLa, RPE1 and HCT116 cell lines (data not shown).

We produced and immunopurified FOR20 anti-peptides antibodies in rabbit and we validated their specificity in immunoblot and immunofluorescence experiments by using competition and siRNA procedures (supplementary material Fig. S3). The FOR20-coding sequence predicts a product of ~20 kDa. In control western blotting experiments, untagged and V5/lumio-tagged FOR20 were expressed in Cos1 cells, and showed reactivity with anti-FOR20 antibodies, at the expected size (Fig. 1D). The anti-FOR20 antibody detected a protein at a size similar to untagged FOR20 expressed in Cos1 cells (~20 kDa), mainly in the Triton X-100-insoluble fraction of RPE1 and HCT116 cells (Fig. 1D). We confirmed that this protein band was FOR20 using two different siRNA to inhibit its expression in RPE1 cells (Fig. 1E). As the related FOP protein mainly localizes at the centrosome, we analyzed purified centrosomes from lymphoblastic KE37 cells by immunoblotting using anti-FOR20 antibodies. Compared with the Triton X-100-soluble fraction, FOR20 was highly enriched in the centrosomal preparation (Fig. 1F).

FOR20 localizes to the centrosomes and pericentriolar satellites

To determine FOR20 localization, we used the rabbit polyclonal antibody previously described and a rat mAb that we also raised (see Materials and Methods section and Fig. 5A for control of its specificity with siRNAs in immunofluorescence assay, and supplementary material Fig. S4 for control of its specificity by competition assay). Both antibodies gave similar results on methanol- or paraformaldehyde-fixed cells. As the rat mAb has a higher sensitivity in immunofluorescence experiments, it was used in all subsequent immunolocalization experiments. We analyzed FOR20 localization at different phases of the cell cycle in RPE1 cells in which centrioles were stably labelled with Centrin1-GFP. In interphase cells, anti-FOR20 antibodies labelled granular structures that were either concentrated around the centrosomes or more scattered in their periphery (Fig. 2). These granular structures were still present in mitotic cells, but were more dispersed in the

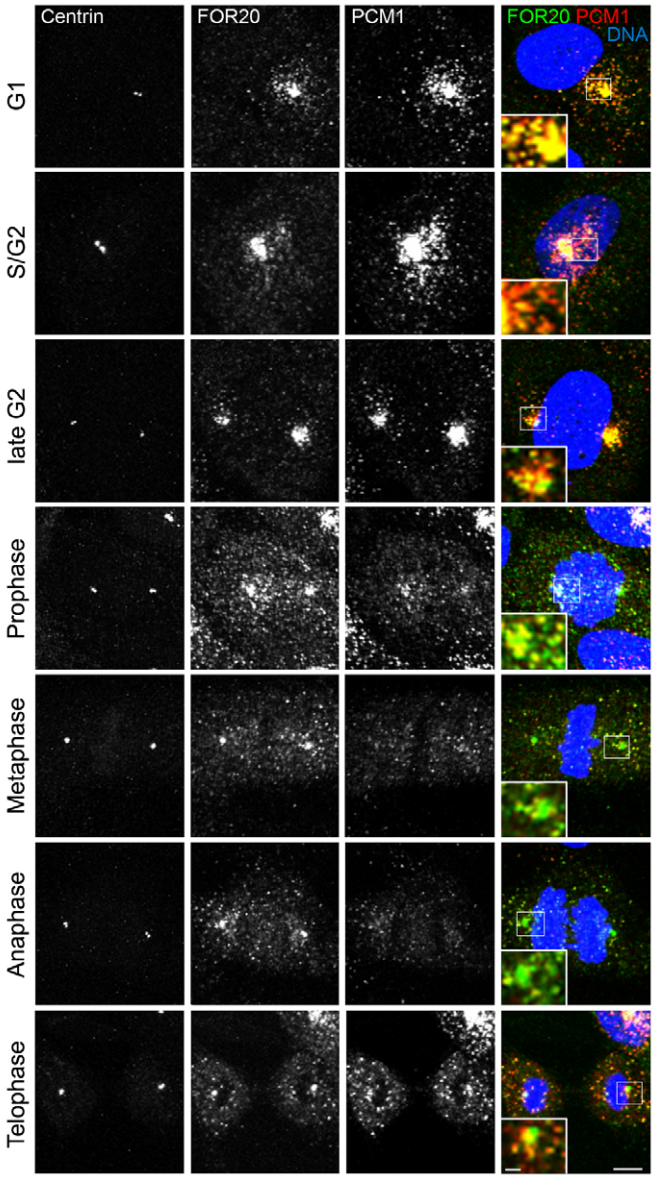

Fig. 2. Subcellular localization of FOR20 during the cell cycle. Asynchronous RPE1 cells stably expressing Centrin1-GFP were fixed in cold methanol and labelled with rat anti-FOR20 and rabbit anti-PCM1 antibodies, and subsequently with Cy3 and Cy5-conjugated anti-rat and anti-rabbit IgG antibodies, respectively. DNA was stained using DAPI (blue). Images from cells at different stages of the cell cycle were recorded. To demonstrate FOR20 and PCM1 colocalization at satellites, we displayed the two proteins in green and red in the merge images, respectively. Bars: 10 μm; 1 μm in insets.

cytoplasm, and there was a strong anti-FOR20 labelling in a focused area around centrioles. These results suggested that FOR20 localizes not only at the centrosome but also in pericentriolar material 1 (PCM1)-enriched pericentriolar satellites (Kubo et al., 1999; Kubo and Tsukita, 2003). Co-detection of PCM1 confirmed FOR20 localization at pericentriolar satellites (Fig. 2). Interestingly, in mitotic cells from prophase to anaphase there was almost no PCM1 localization at the centrosome, in contrast to FOR20. This was also true in two other cell lines (U2OS and KE37, supplementary material Fig. S5A,B). This suggested that FOR20 localization on mitotic centrosomes does not depend on PCM1 and was confirmed by the observation that FOR20 localized on mitotic centrosomes in PCM1-depleted cells (supplementary material Fig. S5C).

The BBS4 protein is present at pericentriolar satellites and participates in ciliogenesis in concert with PCM1 and other BBS proteins (Kim et al., 2004a; Nachury et al., 2007). We used RPE1 cells ectopically expressing a GFP/S-tag BBS4 fusion protein and demonstrated colocalization of FOR20 and BBS4, confirming that FOR20 is a component of pericentriolar satellites (Fig. 3A).

To further characterize FOR20 subcellular localization, we co-labelled FOR20 and PCM1 in pre-embedding immuno-EM experiments on RPE1 cells. Analysis of ultrathin sections showed the presence of FOR20 and PCM1-specific grains on pericentriolar satellites that came out as electron-dense granules of 50-100 nm in size accumulating around centrioles (Kubo et al., 1999) (Fig. 3B).

FOR20 localization complies with microtubule and molecular motor-regulated satellites and depends on its N terminus

To determine how FOR20 localization at centrosomes and satellites is controlled, we carried out a series of experiments. First, we used nocodazole to depolymerize microtubules and examined their role in FOR20 localization. In cells treated with 2 μg/ml nocodazole for 3 hours, FOR20 retained its centrosomal and satellite localization, but satellites were dispersed and tended to form aggregates, as confirmed by PCM1 co-staining (Fig. 4A,i). By contrast, satellites accumulate around the centrosomes in vehicle-treated control cells. This indicated that microtubules participate in satellite distribution but not in the association of FOR20 with satellites and centrosomes.

Second, we studied the role of molecular motors in FOR20 and in satellite localization by transiently overexpressing the cargo-binding region (TPR repeats) of kinesin light chain 1 (KLC1) (Boucrot et al., 2005) and the p50 dynamitin subunit of dynactin (Burkhardt et al., 1997) to inhibit conventional kinesin and dynein activity, respectively. Inhibition of either of the two motors did not prevent FOR20 localization at the centrosome, in contrast to PCM1 (Fig. 4A,ii and iii; supplementary material Fig. S6 for a co-staining with a centrosomal marker). When kinesin was inhibited, we noted an important reduction in the number and size of the puncta in the cytoplasm stained with FOR20 and PCM1. This indicated a decrease in the number and size of satellites co-stained with FOR20 and PCM1 when KLC1 was expressed (Fig. 4A,ii). Long-term inhibition of dynein dispersed satellites, which retained FOR20 and PCM1 labelling (Fig. 4A,iii). Therefore, microtubule integrity and coordinated molecular motor activities are required for the correct localization and the maintenance of pericentriolar satellites. In addition, FOR20 localizes to the centrosome and to satellites, when they are present, independently of microtubules and motors.

Third, we delineated the sequence(s) required for FOR20 centrosome/pericentriolar satellite localization. To achieve this, we constructed expression vectors encoding Myc-tagged wild-type FOR20, various truncation mutants and point mutants at highly conserved residues in the LisH domain and PLL motif (Fig. 4B). All constructs, when expressed at high levels in U2OS cells, showed a diffuse localization in the cytoplasm and nucleus (Fig. 4C and data not shown), except the 1-48 mutant, which showed tubule-like linear and circular structures (Fig. 4C). When cells

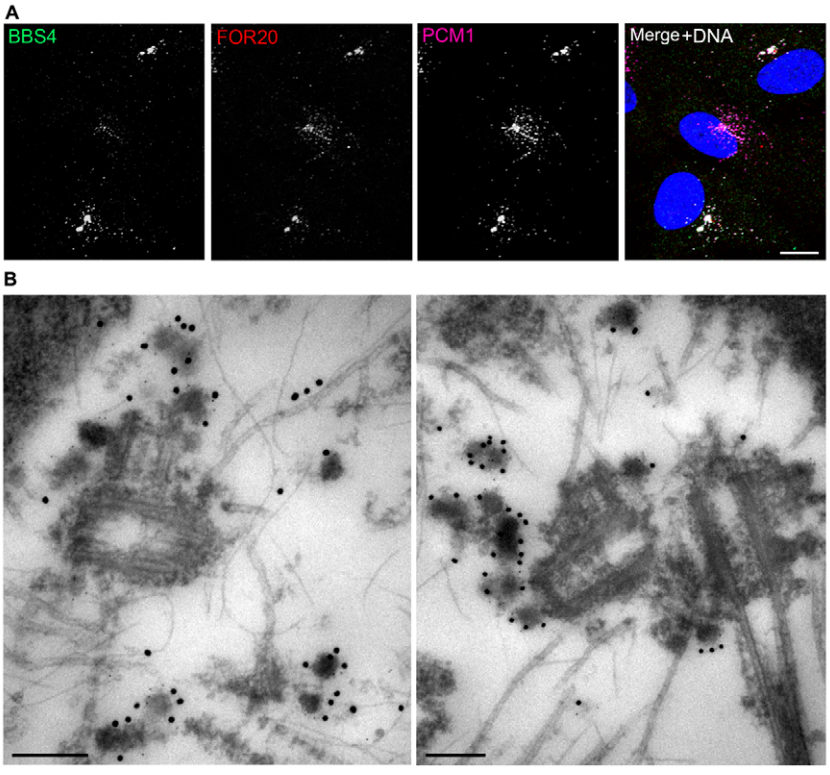

Fig. 3. FOR20 localization at pericentriolar satellites. (**A**) RPE1 cells expressing GFP/S-tag-BBS4 (green) were fixed and labelled with rat anti-FOR20 (red) and rabbit anti-PCM1 (magenta) antibodies. BBS4 expression varies among the cell population, and appears either as small granules resembling normal pericentriolar satellites or as larger aggregates. In all cases, the three proteins colocalized. Scale bar: 10 μm. (**B**) Fixed RPE1 cells were labelled with anti-FOR20 mAb and anti-PCM1 antibodies, and detected with secondary antibodies conjugated to 6 nm and 18 nm colloidal gold, respectively. Cells were then processed for EM. The left picture shows a centrosome with two connected centrioles. In the right picture, two parental centrioles, with one showing axonemal extension, are apposed to growing procentrioles. In both cases, FOR20 and PCM1 are detected around satellites. Bars, 200 nm.

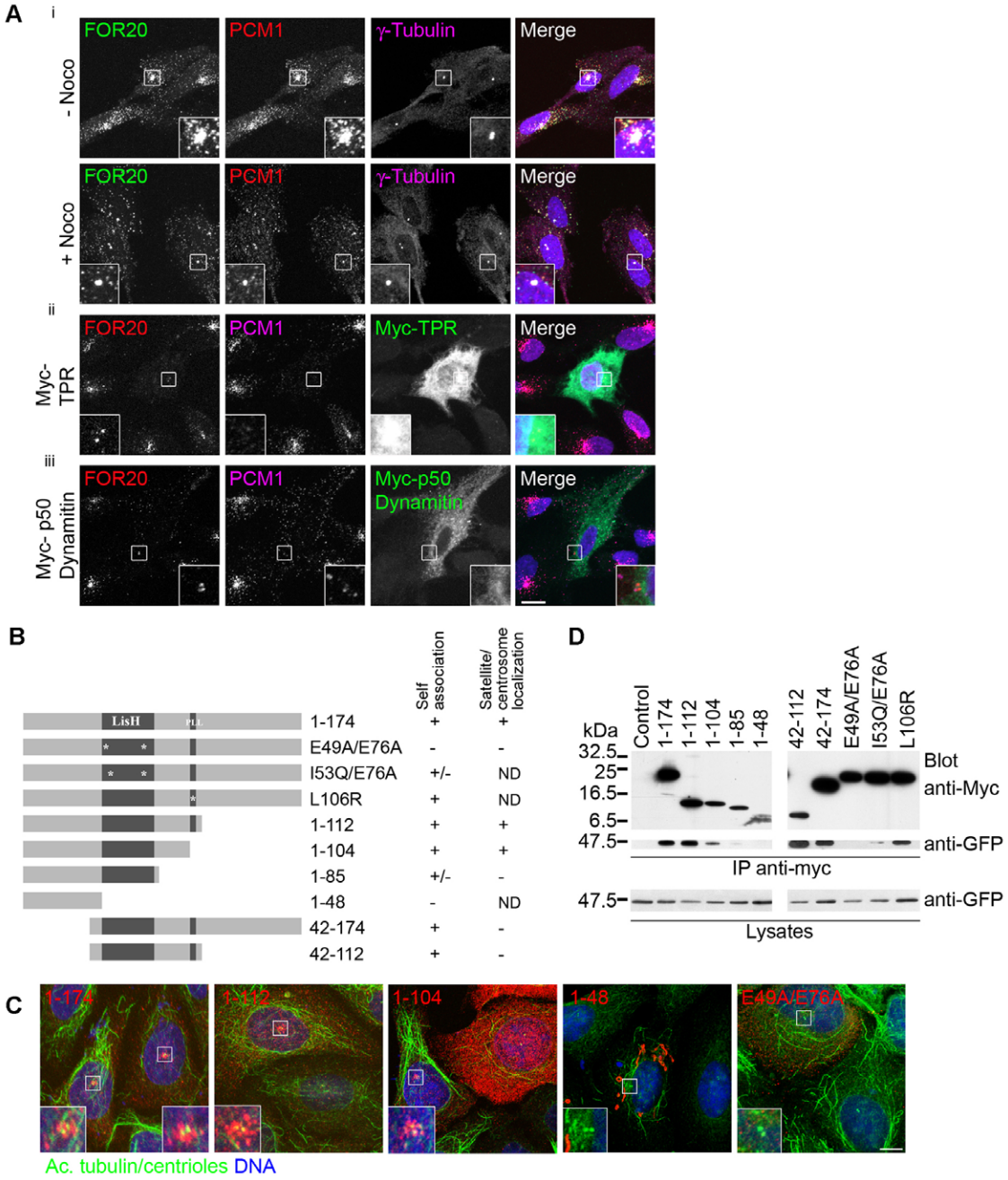

Fig. 4. Factors that regulate FOR20 pericentriolar localization and self-association. (**A**) (i) Asynchronously growing RPE1 cells were incubated or not for 3 hours with 2 µg/ml of nocodazole. Cells were then fixed and labelled with anti-FOR20 (green), anti-PCM1 (red) and anti-γ-tubulin (magenta) antibodies. Merged images include DAPI staining in blue. (ii) RPE1 cells were transfected with an expression plasmid encoding the Myc-TPR motif of KLC1 to inhibit kinesin activity. Cells were fixed 18 hours post transfection and stained with anti-FOR20 (red), anti-PCM1 and anti-Myc (green) antibodies. One transfected cell is shown, surrounded by control, non-transfected cells. FOR20, but not PCM1, persists at the centrosome. (iii) RPE1 cells were transfected with an expression plasmid encoding the Myc-tagged p50 subunit of dynactin to inhibit dynein activity. Cells were fixed 18 hours post transfection and stained as in (ii). The normal staining of FOR20 and PCM1 in untransfected cells is lost in the central cell overexpressing p50 dynamitin. As in (ii), FOR20 but not PCM1 persists at the centrosome when dynein is inhibited. Bar, 10 µm. Insets show centrosomes enlarged. (**B**) Schematic representation of wild type and various FOR20 mutants is depicted. The LisH domain and PLL conserved motif are indicated. On the right of the scheme, + and – recapitulate the localization and self association results shown in Fig. 4C and Fig. 4D. ND: cells with low expression level were never observed for the corresponding constructs, precluding proper interpretation. (**C**) U2OS cells were transiently transfected with expression vectors coding for the indicated Myc-tagged FOR20 constructs. These proteins were detected by immunofluorescence using anti-Myc antibodies (red). Anti-acetylated tubulin staining (green) identifies centrioles in these cells. The pericentriolar region is magnified in insets. A typical centrosome/pericentriolar staining is observed for the 1-174 (full length), 1-112 and 1-104 constructs at low expression levels. Bar, 10 µm. (**D**) Cos1 cells were transfected with a GFP-FOR20 expression vector alone (control lane) or together with various expression vectors coding for the Myc-tagged FOR20 proteins depicted in Fig. 4B. Cell lysates were subjected to immunoprecipitation with anti-Myc agarose beads and immunoprecipitates were resolved by 15% SDS-PAGE. After transfer onto nitrocellulose, the membrane was immunoblotted with anti-Myc and anti-GFP antibodies, as indicated. Aliquots of cell lysates (1/20) were also separated by SDS-PAGE and immunoblotted with anti-GFP antibodies to control the expression of FOR20-GFP in the different transfections (bottom panel).

expressed low levels of ectopic proteins, wild type (1-174), 1-112 and 1-104 truncated protein displayed granular pericentriolar staining (Fig. 4C). We never observed such a distribution in cells expressing 1-85, 42-174, 42-112 truncated mutants and E49A/E76A LisH mutant, whatever their expression levels. These results, recapitulated in Fig. 4B, demonstrate that the first 104 amino acid residues and a functional LisH domain are necessary and sufficient for FOR20 pericentriolar satellite localization.

FOR20 self-associates through a central region, including the LisH domain

The putative capacity of FOR20 to interact with itself was analyzed by co-immunoprecipitation experiments on lysates of transfected Cos1 cells. To achieve this, cells were transiently transfected with expression vectors coding for GFP-tagged FOR20 together with Myc-tagged FOR20 constructs. FOR20-GFP strongly interacted with truncation mutants lacking the first 41 or last 70 amino acid residues (Fig. 4D). Point mutation or deletion of the conserved PLL motif did not preclude self-association of FOR20 in this assay. By contrast, a functional LisH domain is required, as point mutations in this domain strongly diminished or inhibited this association. These co-immunoprecipitation experiments also suggested that residues lying between the LisH domain and PLL motif are involved in self-association. When compared with the sequence required for localization of FOR20 at centrosome/pericentriolar satellites, we can also conclude that self-association is necessary for proper localization of FOR20.

FOR20 regulates pericentriolar satellites distribution

Because PCM1 is a major component of pericentriolar satellites and colocalizes with FOR20 at these structures, we selectively inhibited the expression of each protein using specific siRNAs to determine whether the two proteins depend on each other for correct cellular distribution. When FOR20 was depleted from RPE1 cells, the large accumulation of PCM1 satellites around centrosomes was absent and very few particles were present in this area, whereas PCM1 granules were scattered in the cytoplasm (Fig. 5A). Reciprocally, PCM1 inhibition totally suppressed FOR20 localization at pericentriolar punctate structures, without affecting anti-FOR20 labelling at the centrosome. Importantly, the modification of FOR20 and PCM1 satellites could not be attributed to an alteration of the microtubule network in these experiments, as microtubules retained a normal organization at the steady state and in regrowth experiments (data not shown).

Centrosomes and cytoskeleton-associated proteins show partial solubilization in Triton X-100-containing buffer (Balczon et al., 1999; Black and Kurdyla, 1983; Tassin et al., 1998). Indeed, FOR20 (Fig. 1D; Fig. 5B) and PCM1 (Fig. 5B) were found in both Triton X-100 soluble and insoluble fractions. We believe that this reflects the presence of centrosome and microtubule-associated satellite pools of each protein, together with a non-microtubule associated pool, which is barely detectable in the case of FOR20. The shifted distribution of PCM1 from the insoluble to the soluble fraction upon nocodazole treatment confirmed this hypothesis (Fig. 5B). However, FOR20 remained mainly insoluble after nocodazole treatment, indicating that FOR20 may be loosely associated with satellites. Its insolubility could therefore be explained by its binding to other proteins or structures, including the centrosome itself. This was confirmed by the observation that PCM1 depletion (which induced the loss of satellites) did not prevent FOR20 insolubility (Fig. 5B). Strikingly, PCM1 was found almost exclusively in the Triton X-100 soluble fraction after FOR20 depletion. PCM1 solubility in this case is greater than with nocodazole treatment, probably because large aggregates of satellites form after

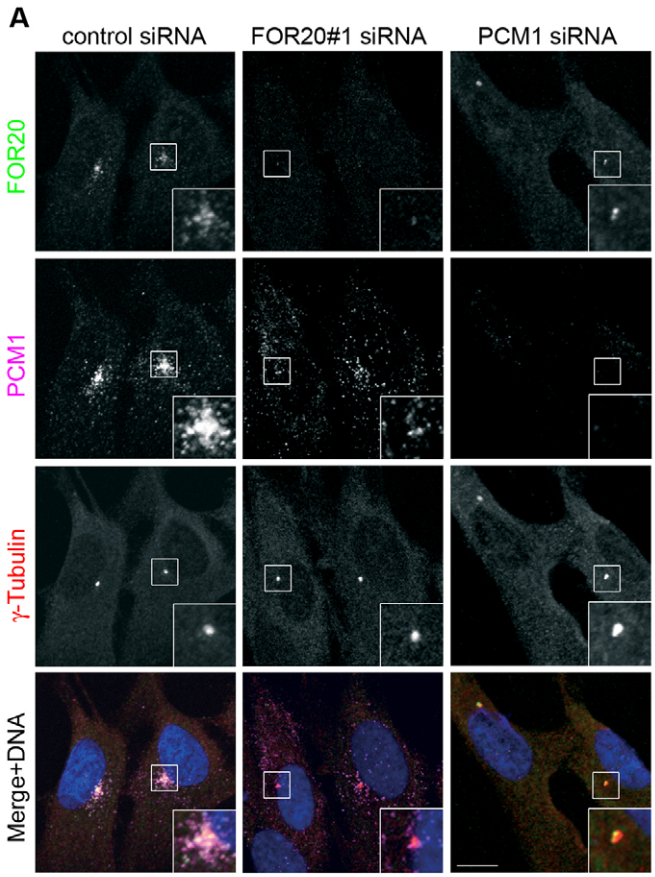

Fig. 5. FOR20 and PCM1 are mutually dependent for their respective subcellular distribution. (**A**) Growing RPE1 cells were transfected with siRNAs for 48 hours and fixed for detection by immunofluorescence of FOR20 (green), PCM1 (magenta) and γ-tubulin (red). We chose to display fields containing two adjacent cells. Insets show magnified images of pericentriolar regions. Note the dispersion of PCM1-labelled satellites in FOR20-depleted cells and restriction of FOR20 localization to centrosomes after treatment with PCM1-specific siRNA. Bar, 10 µm. (**B**) RPE1 cells were treated for 72 hours with the indicated siRNAs or for 3 hours with 2 µg/ml of nocodazole (noco), and subsequently lysed in 1% Triton-X100-containing PHEM buffer. Soluble (SN) and insoluble (P) fractions were collected and similar protein quantities were run on polyacrylamide gel, transferred onto nitrocellulose and blotted with anti-PCM1, FOR20 and γ-tubulin (loading control) antibodies as indicated on the figure.

nocodazole treatment and prevent PCM1 from complete solubilization. The observation of satellite dispersion and the change in PCM1 solubility supports a role for FOR20 in satellite interaction with microtubules.

FOR20 is required for normal ciliogenesis in RPE1 cells

Because we suspected a role for FOR20 in ciliated organisms (see above) and because FOR20 localizes at the basal body and surrounding satellites in ciliated cells (Fig. 6A), we examined the capacity of RPE1 cells to form a primary cilium upon siRNA-mediated FOR20 depletion.

RPE1 cells form a primary cilium in G1, but do so at a higher frequency when induced to quiescence in the absence of serum. We transfected cells twice with siRNAs, in order to obtain long-term FOR20 depletion, and starved cells for 24 hours before fixation. The percentage of ciliated cells, detected by acetylated tubulin staining, was decreased by 36% and 50% after treatment with two different FOR20-specific siRNAs. As a control experiment, PCM1 depletion also led to a decreased percentage of ciliated cells (Fig. 6B), as reported elsewhere (Nachury et al., 2007). Importantly, serum-starved FOR20-depleted cells were negative for KI67 staining, like control cells, which indicated that reduction of cilia frequency was not due to a defect in exiting the cell cycle upon serum starvation caused by FOR20 siRNA (data not shown). Because around half the cells treated with FOR20 siRNA were still ciliated, we next measured the length of their cilia, i.e. measurable nascent or extended acetylated tubulin labelling emerging from one centriole. The measure of acetylated tubulin staining is a reliable marker of cilia length, as checked by the correlation of the fluorescence and DIC (differential interference contrast) images of cilia (data not shown). Remarkably, cells treated with either of the two FOR20-specific siRNA showed a reduction in cilium size of nearly 30% (Fig. 6C). In accordance with this observation, cilium size distribution was strongly shifted to a lower length when FOR20 was inhibited (Fig. 6D). To further document the effect of FOR20 depletion on primary cilium elongation, quiescent cells treated with control or specific siRNA were incubated with high doses of nocodazole to depolymerize axonemal tubulin, nocodazole was then washed out and cells were incubated for 24 hours in serum-free medium to allow cilium regrowth. A measure of cilia length during this time course showed that the growth kinetic of the primary cilium was affected by FOR20 depletion. In FOR20 siRNA-treated cells, cilia length rapidly reached a plateau 6 hours after nocodazole washout at a mean size of around 2 μm, in contrast to control cilia that grow for 24 hours before reaching a plateau at a mean size of 4 μm. Longitudinal sections of primary cilia observed by transmission electron microscopy (TEM) showed the presence of a basal body docked at the cell cortex and an associated daughter centriole in control and FOR20-depleted cells (Fig. 6F). No gross alteration was detected in basal body and axoneme structure in cells treated with anti-FOR20 siRNA (number of cells observed: control siRNA, n=3; FOR20 siRNA, n=6).

To support a putative role for FOR20 in cilium biogenesis in vivo, we took advantage of the cross-reactivity of our rat monoclonal antibody with mouse FOR20 (supplementary material Fig. S7) to immunolabel tissue sections of adult mouse trachea. Fig. 6G shows that FOR20 localizes close to basal bodies at the base of cilia. Interestingly, we also observed FOR20 staining along the cilia itself. Therefore, FOR20 may have a role not only in immotile primary cilia, but also in the regulation of motile cilia at the surface of multiciliated epithelia. In conclusion, FOR20 has a close link with cilia in cells and tissues, and its depletion induces either a complete inhibition of ciliogenesis or a reduction in the length of cilia.

Discussion

Cilia and flagella are unique features of many eukaryotic cells that serve diverse functions in protists and in animal cells. Ciliated organisms are endowed with genes encoding highly conserved proteins required for cilium formation, in particular proteins belonging to the IFT and BBSome complexes.

Structural and phylogenetic features of FOR20

We have identified a protein that is found in most ciliated organisms and is absent from non-ciliated ones. This protein, named FOR20, is related to FOP (Acquaviva et al., 2009; Popovici et al., 1999), and more distantly to OFD1 (Ferrante et al., 2006; Romio et al., 2004). In vivo, deficiencies in OFD1 and FOP promote ciliopathic syndromes (Ferrante et al., 2001; Ferrante et al., 2006) (C.A. and O.R., unpublished), suggesting that FOR20 may also regulate cilium formation. In contrast to FOP and FOR20, OFD1 is present only in vertebrates and has probably evolved late in evolution to fulfil specific functions in vertebrate cilia. Further supporting a putative role of FOR20 in ciliogenesis, its orthologue in the ciliate *T. thermophila* was recently identified as a basal body-associated BBC20 protein (Kilburn et al., 2007). We have also identified a partial predicted cDNA encoding a FOR20 orthologue in the fungus *B. dendrobatidis*, but none in other fungi. This is of interest as *B. dendrobatidis* exists as a uniflagellated zoospore during its life cycle, in contrast to other fungi.

FOR20, like FOP and OFD1, has a LisH domain in its N-terminal region, which is known to mediate homodimerization in LIS1 and FOP (Kim et al., 2004b; Mikolajka et al., 2006). In agreement, we showed that this domain is also necessary to mediate FOR20 self-interaction. A PLL motif, which lies in a C-terminal position relative to the LisH domain, is highly conserved in FOR20 and FOP. This PLL motif forms intermolecular contacts with two conserved residues of the LisH domain, and is expected to participate in dimerization (Mikolajka et al., 2006). However, deletion or a point mutation of PLL in FOR20 indicates that this motif is not strictly required for self-association. It may only be necessary to increase the stability of the interaction. This motif is not conserved in OFD1, LIS1 or other LisH domain-containing proteins, confirming that it is not strictly necessary for dimer formation. Interestingly, a tyrosine residue highly conserved in FOR20 orthologues is appended at the C terminus of the PLL motif (see Fig. 1), and may be subjected to phosphorylation to modulate intermolecular interactions.

The N-terminal part of the protein preceding the LisH domain is also well conserved in FOR20 orthologues and shows similarities to FOP and OFD1 N-termini. This region was named the TOF (Tonneau, OFD1, FOP) motif in a recent study characterizing Tonneau1, the FOP orthologue in land plants (Azimzadeh et al., 2008). Its role is unknown, but we show here that it is required, together with the LisH domain, to address FOR20 to pericentriolar satellites and centrosomes.

FOR20, satellites and primary cilium

FOR20 has a specific subcellular distribution at both the centrosome and PCM1-enriched pericentriolar satellites (also named PCM1 granules) in RPE1 interphasic cells. Satellites are described in

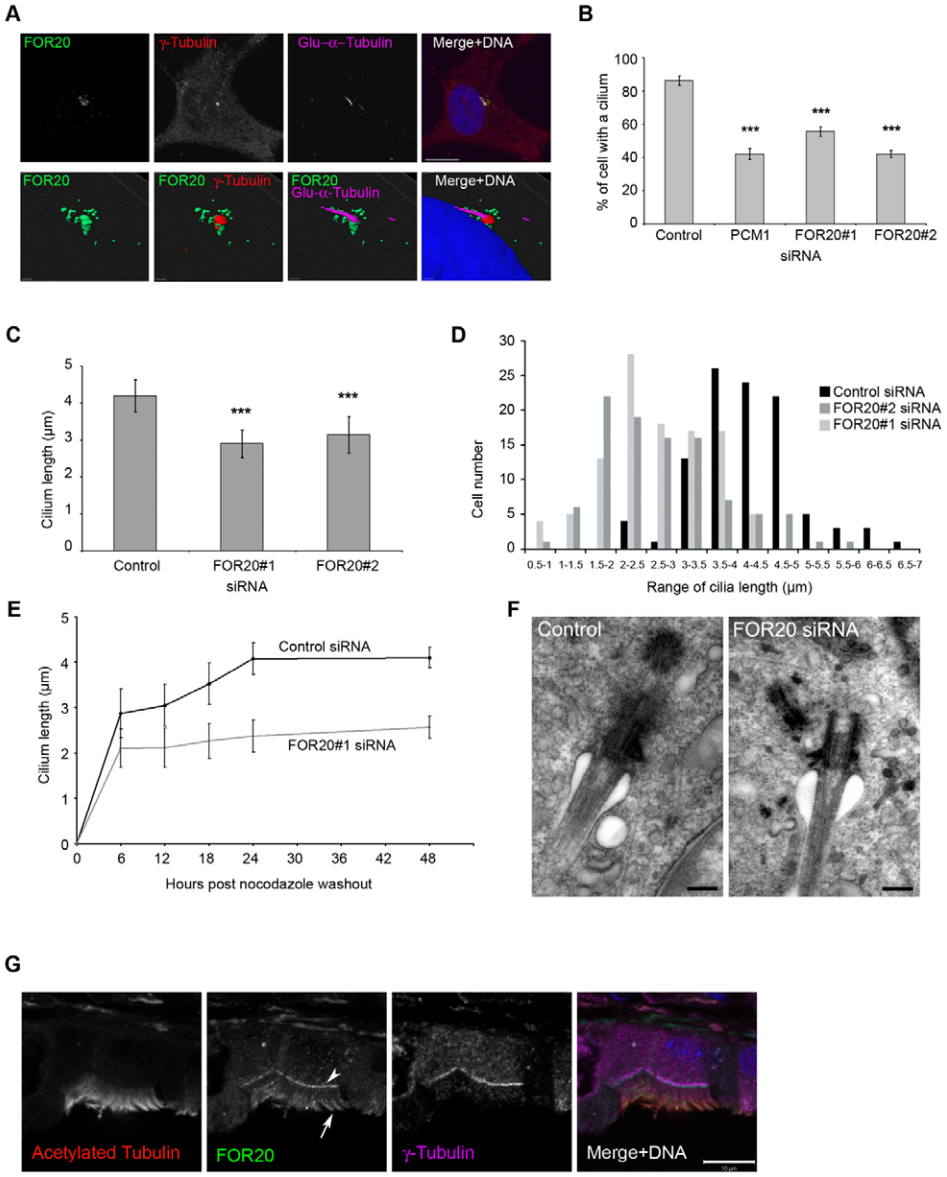

Fig. 6. FOR20 controls ciliogenesis. (**A**) Serum-starved RPE1 cells were fixed and labelled with anti-FOR20 (green), anti γ-tubulin (red, marks the centrosome) and anti-detyrosinated α-tubulin (Glu-α-Tubulin, magenta, marks the cilium). The upper panel shows a projected image of 0.04 μm stack acquisitions. The bottom panel shows a 3D reconstruction using the 3D surface view software AMARIS (Bitplane AG) with a perspective/view from left corner of the 2D picture shown in the top panel. Both views clearly show that FOR20 localizes at the pericentriolar satellites and basal body of ciliated cells. Bar, 10 μm. (**B**) Cells treated with the indicated siRNA were serum starved for 24 hours and labelled with anti-acetylated tubulin antibody to detect cells with a primary cilium. The percentage of ciliated cells was calculated from the observation of 200 cells per experiment, and we show the mean percentage from five independent experiments. Vertical bars indicate standard deviation (s.d.). *P* values compared with the control were calculated using unpaired Student's *t*-tests. ***$P<0.001$. (**C**) Cells were treated as in B and, whenever a cilium was present, we measured the length of the ciliary axoneme labelled with anti-acetylated tubulin antibody. Around 100 measurements were made under each experimental condition and the mean value from one out of five independent experiments is reported, along with the s.d. (vertical bars). ***$P<0.001$ compared with the control. (**D**) RPE1 cells were treated and the cilia/axonemes were measured as in C. The distribution of axoneme/cilia length from one out of three independent experiments is shown. There is a leftward shift in the length distribution from FOR20 siRNA-treated cells compared with the control. (**E**) The length of cilia growing after nocodazole treatment was measured at different time points after nocodazole washout (see Materials and Methods) in control and FOR20 siRNA-treated cells. 100 measurements were made for each condition and the mean value is plotted together with the s.d. (**F**) Representative image of a TEM acquisition of longitudinal section of a primary cilium from control (left) or FOR20 siRNA (right)-treated RPE1 cells. Bars, 200 nm. (**G**) Cryosection of paraformaldehyde-fixed mouse trachea labelled with mouse anti-acetylated tubulin (red), rat anti-FOR20 (green) and rabbit anti-γ-tubulin (magenta) antibodies. Anti-FOR20 not only labels the basal region of the cilia (arrow), but also the cilia themselves (arrowhead). Bar, 10 μm.

several species, including yeast, *Drosophila* and vertebrates (Dammermann and Merdes, 2002; Kubo et al., 1999; Kubo and Tsukita, 2003; Megraw et al., 2002; Sawin et al., 2004). They are defined as small and dynamic granular entities composed of proteins involved in centrosome and microtubules nucleating functions. In vertebrate cells, PCM1 satellites are more precisely defined as

electron dense round structures 50-100 nm in size (Kubo et al., 1999). A number of cytoplasmic PCM1 granules are not co-labelled by anti-FOR20 antibodies. This could be due to the existence of different kinds of satellites, to a difference in PCM1 and FOR20 protein abundance or distribution, or to experimental conditions (e.g. a differential sensitivity in PCM1 and FOR20 detection). Remarkably, in mitotic cells, FOR20 satellites are more dispersed and there is an intense labelling at the centrosome, which is in sharp contrast to PCM1 staining, particularly in metaphase and anaphase, when PCM1 granules disappear (Fig. 2) (Kubo and Tsukita, 2003). The localization of these two proteins is therefore differentially regulated, and they may not form stable complexes. Indeed, we were not able to show co-immunoprecipitation of PCM1 and FOR20 (data not shown). However, it is clear that the correct localization of each of these proteins is mutually dependent. Depletion of FOR20 induces a dispersion of PCM1 satellites in the cytoplasm and, reciprocally, depletion of PCM1 abolishes FOR20 localization in satellites but does not affect its centrosomal localization. PCM1 depletion may induce the complete loss of pericentriolar satellites per se, which could explain the absence of granular staining by anti-FOR20 antibody. Indeed, PCM1 is probably an essential core structure protein of satellites, as it was proposed from experiments in which overexpressed PCM1 formed aggregates mimicking large pericentriolar satellites which dissociate in mitosis (Kubo and Tsukita, 2003). As a consequence of FOR20 depletion, PCM1-labelled granules are not lost but dispersed throughout the cytoplasm. Satellites normally move along the microtubules and their dynamic behaviour depends on microtubules in several ways. In *Drosophila*, satellites enriched in centrosomal proteins CNN and TACC, show back and forth movements (flares) that probably depend on astral microtubules dynamics (Megraw et al., 2002). PCM1 satellites in vertebrates can also move in vivo towards the centrosome or towards the cell periphery (Kubo et al., 1999). The role of dynein in satellite movements towards the minus-end of microtubules has been shown on reconstituted asters (Kubo et al., 1999), and dynein inhibition has also been shown to result in the dispersion of PCM1 granules (Dammermann and Merdes, 2002). As expected, we observed that dynactin (dynein activator) inhibition results in the dispersion of FOR20 and PCM1-co-labeled satellites in the cell cytoplasm. On the other hand, inhibition of conventional kinesin activity results in a large decrease in the number and size of satellites. This result can be explained by a possible requirement for plus-end directed transport to recycle satellites, in agreement with the observation that satellites can also move towards the cell periphery (Kubo et al., 1999). In the absence of such an ‘anterograde’ transport, satellite components may be dissociated, or even degraded, at the centrosome, which is known to concentrate the proteasome and associated regulatory proteins (Fabunmi et al., 2000). In support of this hypothesis, a recent study (Didier et al., 2008) has demonstrated the accumulation of PCM1 and ubiquitinated centrosomal proteins at the centrosome upon inhibition of proteasome activity.

FOR20 depletion, like microtubules depolymerization and dynein inhibition, induces satellite scattering and PCM1 enrichment in the Triton X-100 soluble fraction (Fig. 5B). This suggests that FOR20 regulates a microtubule-dependent process, either directly or indirectly. However, we did not detect any binding of recombinant FOR20 to purified microtubules in vitro (data not shown). Two proteins, BBS4 and HAP1, bind both PCM1 and the p150^{Glued} subunit of dynactin, and it has been suggested that they act as adaptors to connect PCM1 satellites to the dynein-dynactin complex (Engelender et al., 1997; Kim et al., 2004a). FOR20 may thus be required to promote stable interaction of PCM1/dynein-dynactin complexes with microtubules. This is in line with the fact that the LisH domain may contribute to microtubule dynamics regulation, either by its dimerization properties and/or by dynein or microtubule binding (Emes and Ponting, 2001). Further experiments are required to explain the role of FOR20 in satellites binding and/or movements along microtubules.

PCM1 function in ciliogenesis is supposed to be linked to the role of pericentriolar satellites in this process. Compared with PCM1, FOR20 additionally has a strong centrosomal localization that is independent of its satellite localization. This observation is important regarding the effect of FOR20 depletion on primary cilium formation in RPE1 cells: ciliogenesis defects could be due to two non-exclusive mechanisms. First, the perturbation of pericentriolar satellites by FOR20 depletion is likely to affect the recruitment at the centrosome and at the basal body of proteins important for ciliogenesis, as it has been proposed for PCM1. However, depletion of FOR20 did not affect the centrosomal localization of γ-tubulin (Fig. 5), CEP250, centrin, pericentrin, FOP, CEP215 and EB1 (data not shown). It will be important to look carefully at the localization of other proteins, such as IFT and BBS proteins, in FOR20-depleted cells. Second, FOR20 may function at the basal body to directly regulate ciliogenesis. Interestingly, BBC20, the *Tetrahymena* FOR20 orthologue, localizes exclusively at the side of the basal body transition zone, suggesting that it may participate in protein sorting and/or IFT loading at the base of cilia (Kilburn et al., 2007). This is a possible explanation for cilia shortening or absence in RPE1 cells with decreased or null FOR20 expression. This explanation also fits well with our kinetics of cilium growth (Fig. 6E), in which the limited growth rate may be explained by abnormal loading of cilia components at the transition zone. The localization of FOR20 at the transition zone, like its orthologue BBC20, has to be confirmed in vertebrate cells. In our TEM experiments, we were not able to detect FOR20 at centrosomes and basal bodies with enough efficiency to define precisely its position on these organelles. This is probably explained by technical limitations. Addressing this issue will require technical improvement and should be completed by TEM experiments on thin sections of mouse ciliated tissues.

Neural tube defect is one feature of ciliary dysfunction syndromes (Badano et al., 2006), and brain defects such as hydrocephaly and microcephaly can result, respectively, from mutation in genes that regulate motile cilia (Lechtreck et al., 2008; Town et al., 2008) and centrosome-driven asymmetric division (Bond and Woods, 2006). Interestingly, the human *FOR20* gene lies within the minimal critical region of 8 cM defined in the microhydranencephaly genetic disorder (Kavaslar et al., 2000). However, sequencing the *FOR20* exons and parts of introns revealed single nucleotide polymorphisms (SNPs) reported in databases but no novel sequence variant suggestive of a gene mutation in DNA from patients (data not shown). Other ciliopathy-affected patient candidates will be tested for potential *FOR20* mutations.

Among the proteins necessary for ciliogenesis, FOR20, like most of the IFT and BBSome components, is present in a wide range of ciliated eukaryotes, in contrast to proteins such as PCM1 that appeared late in the course of evolution. The IFT and possibly the BBSome complexes could have evolved from vesicles coats, using proteins based on WD40 and TPR modules (Jekely and Arendt, 2006). We suggest that the LisH domain, together with the

conserved N-terminal TOF region (Azimzadeh et al., 2008), may also constitute an ancestral module required for the biogenesis of motile and immotile cilia. Consequently, a better knowledge of FOR20 roles will prove important for understanding the mechanism of cilia formation in many living organisms, and the *FOR20* gene constitutes a putative target for mutations in ciliopathies.

Materials and Methods

Sequence alignment and phylogenetic analysis

Sequences were aligned using the MUSCLE algorithms (Edgar, 2004) and edited manually using SeaView (Galtier et al., 1996). Phylogenetic analyses were carried out using the PHYLIP package (Felsenstein, 1989) (distance and parsimony algorithms) or phyml (Guindon and Gascuel, 2003) (maximum likelihood algorithm). A total of 1000 bootstrap replicates were done.

Northern blot hybridization

A commercial northern blot loaded with 2 μg of polyadenylated RNAs extracted from various human tissues (Origene) was hybridized 15 hours at 42°C in UltraHyb buffer (Ambion) with a probe corresponding to the coding region of the *FOR20* cDNA. This probe was radiolabelled with α^{32}P-dCTP by the random priming method. The membrane was subsequently washed twice in 2×SSC, 0.1% SDS at 42°C and twice in 0.25×SSC, 0.1% SDS at 65°C before autoradiographic exposure.

Cells, antibodies and reagents

RPE1 cells were grown in DMEM/F12 (Invitrogen) supplemented with 10% FCS (heat-inactivated 30 min at 56°C), 10 U/ml penicillin, 10 μg/ml streptomycin. RPE1 cells expressing GFP/S-tag BBS4 (LAP-BBS4) (a gift from M. Nachury, Stanford University) and RPE1/Centrin1-GFP were grown in the same medium as RPE1. COS1, HCT116 and KE67 cells were grown in DMEM, McCoy's 5A and RPMI, respectively, with similar supplements as above.

Anti-human FOR20 monoclonal antibody was obtained following immunization of rats with a GST-FOR20 fusion protein. Immune spleen cells were fused with the non-secreting myeloma X63-Ag8.653 cells and grown in selective medium. Hybridoma supernatants were first screened by ELISA on GST-FOR20 and GST alone. GST-FOR20-only positive populations were screened by immunofluorescence on methanol-fixed RPE1 cells and western blotting of lysates from Cos1 cells overexpressing Myc-tagged FOR20. Selected clones were cloned three times before large-scale antibody production. The 17E2 mAb was selected for use in this study. Of note, this anti-FOR20 mAb does not detect endogenous FOR20 in western blot experiment because of low sensitivity in this assay.

Anti-human FOR20 polyclonal antibody was obtained by rabbit immunization with the peptide PSRRKPMDDHLRKEE (amino acids 143-157) conjugated to keyhole limpet haemocyanin and affinity purification (Eurogentec). Anti-Myc mAb 9E10 was purchased from Santa-Cruz Biotechnology. Mouse mAbs anti-α-tubulin (clones B-5-1-2 and DM1-A), anti-acetylated tubulin (clone 6-11B-1), anti-γ-tubulin (clone GTU-88) and rabbit polyclonal anti-γ-tubulin (T3559) antibodies were obtained from Sigma. Mouse mAbs anti-GFP (clones 7.1 and 13.3) were from Roche. Rabbit anti-detyrosinated α-tubulin (AB3201) was from Millipore. Rabbit anti-PCM1 antibodies (A301-149A, A301-150A) were obtained from Bethyl Laboratories. Rabbit and mouse polyclonal antisera against PCM1 used in initial experiments were a kind gift from A. Merdes (Institut Pierre Fabre, Toulouse, France).

A plasmid containing the full-length *FOR20* cDNA sequence (IMAGE clone 4702249) and an expression construct in pReceiver-M06 vector coding for FOR20 sequence fused to GFP at its C terminus were obtained from RZPD (Berlin, Germany).

Plasmids construction and mutagenesis

The sequence coding for the full-length and truncated FOR20 proteins were amplified by PCR using Platinum HiFi polymerase (Invitrogen) and Gateway compatible primers and transferred into pDONR/ZEO using Gateway technology-mediated recombination. The sequences were subsequently transferred by Gateway recombination into a modified Gateway-compatible pRK5/Myc expression vector. Point mutations were introduced in the FOR20 coding sequence by mean of the Stratagene Quickchange II or Multisite kits, following manufacturer instructions.

Immunofluorescence

Cells grown on coverslips were fixed in methanol at –20°C for 6 minutes and rinsed in PBS. After blocking in PBS, 0.1% or 3% BSA, cells were incubated with primary antibodies diluted in PBS-BSA for 30 to 45 minutes. After washing in PBS, 0.1% Tween20, primary antibodies were detected using anti-Ig secondary antibodies conjugated to cyanines (Cy2, Cy3, Cy5) from Jackson Laboratories or Alexa Fluor (Alexa Fluor 488 and 647) from Invitrogen. DNA was stained with 250 ng/ml DAPI for 2 minutes. Cells were mounted in Prolong Gold anti-fade reagent (Invitrogen) and examined on an LSM-510 Carl Zeiss confocal microscope with a ×63 NA1.4 Plan Apochromat objective. *Z*-series optical sections were obtained at 0.3 μm steps, unless otherwise stated in the legend, and then projected with LSM software (Zeiss) as maximum projections. Images were processed using Photoshop 8.0.1.

Immunofluorescence on tissue sections

Trachea were collected from adult 129/B6 mice (15 weeks old), fixed in 4% paraformaldehyde overnight at 4°C, rinsed in PBS, incubated in 30% sucrose overnight at 4°C, included and frozen in OCT embedding matrix (Cellpath). Cryosections (12 μm) were obtained on a Leica CM30505S cryotome and processed for immunohistochemistry. Slides were rehydrated in PBS, permeabilised for 10 minutes in PBS/0.2% Triton X-100, rinsed in PBS and saturated for 30 minutes in PBS, 3% BSA. Slides were incubated in the same buffer with rat anti-FOR20 antibody (1/10,000), anti-acetylated tubulin antibody (1/2000), anti-γ-Tubulin (1/2000) for 90 minutes, rinsed in PBS, incubated 2 hours with Alexa Fluor-coupled secondary antibodies (Invitrogen, 1/2000) and 250 ng/ml DAPI. Slides were rinsed in PBS and mounted in Prolong Gold mounting medium (Invitrogen) before observation on a LSM-510 Carl Zeiss confocal microscope with a ×63 NA1.4 Plan Apochromatic objective.

Immunoelectron microscopy

Cells grown on Lab-Tek permanox Chamber were permeabilized 6 minutes in PEM 0.25% Triton and were prefixed in PEM 0.25% glutaraldehyde 10 minutes at room temperature. After three washes in PBS containing 0.1% BSA and 0.1% Tween, the cells were incubated with anti-FOR20 (1/20,000) and anti-PCM1 (1/1000) antibodies for 1 hour. The cells were washed three times with PBS containing 0.1% BSA and 0.1% Tween 20, and were incubated with goat anti-rat antibody conjugated to 6 nm colloidal gold (1/40; Jackson Laboratories) and goat anti-rabbit antibody conjugated to 18 nm colloidal gold (1/40; Jackson Laboratories) for 1 hour. For electron microscopy cells were fixed with 2.5% glutaraldehyde and processed for dehydration and embedding, as described previously (Acquaviva et al., 2009).

Centrosome preparation

Centrosomes were isolated from KE-37 cells as previously described (Bornens et al., 1987). Purified centrosomes were used for centrosomal protein extracts after centrifugation, solubilization in 1% SDS buffer and sonication.

Cell transfection

Cells were transfected with plasmids using Fugene 6 reagent (Roche Applied Science) according to the manufacturer's instructions. For siRNA experiments, two oligonucleotides were synthesized corresponding to nucleotides 178-196 GAGAGTATTTAGAATTCAA, siRNA#1) and 1054-1072 (GTATTATAAAGG-CCCTTAA siRNA#2) of human *FOR20*. The sequence of *PCM1*-specific siRNA has been published (siRNA PCM-1.2) (Srsen et al., 2006). siRNA transfections were carried out in OptiMEM using Oligofectamine (Invitrogen), according to the manufacturer's instructions. The day before transfection, 50,000 RPE1 cells were seeded in six-well plates containing coverslips. Cells were transfected a second time 48 hours after the first transfection, before additional incubation, methanol fixation and processing for immunofluorescence.

Immunoprecipitation and western blot analysis

Cos1 cells were washed in PBS and lysed in 20 mM Tris-HCl (pH 7.5), 2 mM EDTA, 150 mM NaCl, 1% Igepal CA630 (Sigma) plus a Complete Protease Inhibitor Cocktail (Roche Applied Science) buffer on ice. After centrifugation for 20 minutes at 13,000 rpm at 4°C, cleared lysates were obtained. For immunoprecipitation, extracts were incubated with agarose beads conjugated to anti-Myc antibodies (Santa Cruz Biotechnology) for 3 hours at 4°C. Beads were pelleted and washed five times with lysis buffer. Samples were separated using in house SDS-PAGE or NuPAGE 4-12% Novex Bis-Tris gels according to the manufacturer's instructions (Invitrogen).

Triton-X100 soluble and insoluble fractions were obtained as follows: cells were washed in PBS, lysed in PHEM buffer [45 mM PIPES, 45 mM HEPES, 10 mM EGTA, 5 mM $MgCl_2$ (pH 6.9)] plus 1% Triton X-100 and protease inhibitors and centrifuged at 400 ***g*** for 45 minutes. The supernatant was collected (soluble fraction) and the pellet was washed in PHEM alone and solubilized in 1% SDS containing buffer (insoluble fraction) and sonicated.

Cell extracts separated on polyacrylamide gels were transfered onto Hybond-C membrane (GE Healthcare Life Science) followed by detection with antibodies.

Primary cilium regrowth assay

After siRNA transfection, cells were maintained in serum-free medium for 12 hours to induce primary cilium formation. Cells were then treated with 33 μM nocodazole for 6 hours to depolymerize cytoplasmic and axonemal microtubules. Cells were fixed at 0, 6, 12, 18, 24 and 48 hours after nocodazole removal. As a marker of axoneme length, we immunostained acetylated tubulin and measured the length of the cilia in Axiovision software.

We thank A. Merdes for anti-PCM1 antibodies, M. Nachury for the LAP-BBS4-expressing RPE1 cells, S. Meresse for p50 dynamitin and KLC1-TPR expression plasmids, and M. Bornens for the Centrin1-GFP plasmid. We acknowledge A. Bole and S. Fatah (Centre d'Immunologie de Marseille-Luminy) for help in monoclonal antibody production, and O. Cabaud for technical assistance. We are also indebted to M. Leroux for interesting discussions. This work was

supported by INSERM and Institut Paoli-Calmettes. F.S. is a recipient of a fellowship from the Ministère de la Recherche et de l'Enseignement Supérieur.

Supplementary material available online at
http://jcs.biologists.org/cgi/content/full/123/14/2391/DC1

References

Acquaviva, C., Chevrier, V., Chauvin, J. P., Fournier, G., Birnbaum, D. and Rosnet, O. (2009). The centrosomal FOP protein is required for cell cycle progression and survival. *Cell Cycle* **8**, 1217-1227.

Azimzadeh, J., Nacry, P., Christodoulidou, A., Drevensek, S., Camilleri, C., Amiour, N., Parcy, F., Pastuglia, M. and Bouchez, D. (2008). Arabidopsis TONNEAU1 proteins are essential for preprophase band formation and interact with centrin. *Plant Cell* **20**, 2146-2159.

Badano, J. L., Mitsuma, N., Beales, P. L. and Katsanis, N. (2006). The ciliopathies: an emerging class of human genetic disorders. *Annu. Rev. Genomics Hum. Genet.* **7**, 125-148.

Balczon, R., Varden, C. E. and Schroer, T. A. (1999). Role for microtubules in centrosome doubling in Chinese hamster ovary cells. *Cell Motil. Cytoskeleton* **42**, 60-72.

Black, M. M. and Kurdyla, J. T. (1983). Microtubule-associated proteins of neurons. *J. Cell Biol.* **97**, 1020-1028.

Blacque, O. E., Reardon, M. J., Li, C., McCarthy, J., Mahjoub, M. R., Ansley, S. J., Badano, J. L., Mah, A. K., Beales, P. L., Davidson, W. S. et al. (2004). Loss of C. elegans BBS-7 and BBS-8 protein function results in cilia defects and compromised intraflagellar transport. *Genes Dev.* **18**, 1630-1642.

Bond, J. and Woods, C. G. (2006). Cytoskeletal genes regulating brain size. *Curr. Opin. Cell Biol.* **18**, 95-101.

Bornens, M., Paintrand, M., Berges, J., Marty, M. C. and Karsenti, E. (1987). Structural and chemical characterization of isolated centrosomes. *Cell Motil. Cytoskeleton* **8**, 238-249.

Boucrot, E., Henry, T., Borg, J. P., Gorvel, J. P. and Meresse, S. (2005). The intracellular fate of Salmonella depends on the recruitment of kinesin. *Science* **308**, 1174-1178.

Burkhardt, J. K., Echeverri, C. J., Nilsson, T. and Vallee, R. B. (1997). Overexpression of the dynamitin (p50) subunit of the dynactin complex disrupts dynein-dependent maintenance of membrane organelle distribution. *J. Cell Biol.* **139**, 469-484.

Christensen, S. T., Pedersen, S. F., Satir, P., Veland, I. R. and Schneider, L. (2008). The primary cilium coordinates signaling pathways in cell cycle control and migration during development and tissue repair. *Curr. Top. Dev. Biol.* **85**, 261-301.

Dammermann, A. and Merdes, A. (2002). Assembly of centrosomal proteins and microtubule organization depends on PCM-1. *J. Cell Biol.* **159**, 255-266.

Dawe, H. R., Farr, H. and Gull, K. (2007). Centriole/basal body morphogenesis and migration during ciliogenesis in animal cells. *J. Cell Sci.* **120**, 7-15.

Deane, J. A., Cole, D. G., Seeley, E. S., Diener, D. R. and Rosenbaum, J. L. (2001). Localization of intraflagellar transport protein IFT52 identifies basal body transitional fibers as the docking site for IFT particles. *Curr. Biol.* **11**, 1586-1590.

Didier, C., Merdes, A., Gairin, J. E. and Jabrane-Ferrat, N. (2008). Inhibition of proteasome activity impairs centrosome-dependent microtubule nucleation and organization. *Mol. Biol. Cell* **19**, 1220-1229.

Edgar, R. C. (2004). MUSCLE: multiple sequence alignment with high accuracy and high throughput. *Nucleic Acids Res.* **32**, 1792-1797.

Emes, R. D. and Ponting, C. P. (2001). A new sequence motif linking lissencephaly, Treacher Collins and oral-facial-digital type 1 syndromes, microtubule dynamics and cell migration. *Hum. Mol. Genet.* **10**, 2813-2120.

Engelender, S., Sharp, A. H., Colomer, V., Tokito, M. K., Lanahan, A., Worley, P., Holzbaur, E. L. and Ross, C. A. (1997). Huntingtin-associated protein 1 (HAP1) interacts with the p150Glued subunit of dynactin. *Hum. Mol. Genet.* **6**, 2205-2212.

Fabunmi, R. P., Wigley, W. C., Thomas, P. J. and DeMartino, G. N. (2000). Activity and regulation of the centrosome-associated proteasome. *J. Biol. Chem.* **275**, 409-413.

Felsenstein, J. (1989). PHYLIP-Phylogeny Inference Package (Version 3.2). *Cladistics* **5**.

Ferrante, M. I., Giorgio, G., Feather, S. A., Bulfone, A., Wright, V., Ghiani, M., Selicorni, A., Gammaro, L., Scolari, F., Woolf, A. S. et al. (2001). Identification of the gene for oral-facial-digital type I syndrome. *Am. J. Hum. Genet.* **68**, 569-576.

Ferrante, M. I., Zullo, A., Barra, A., Bimonte, S., Messaddeq, N., Studer, M., Dolle, P. and Franco, B. (2006). Oral-facial-digital type I protein is required for primary cilia formation and left-right axis specification. *Nat. Genet.* **38**, 112-117.

Galtier, N., Gouy, M. and Gautier, C. (1996). SEAVIEW and PHYLO_WIN: two graphic tools for sequence alignment and molecular phylogeny. *Comput. Appl. Biosci.* **12**, 543-548.

Gerdes, J. M. and Katsanis, N. (2008). Ciliary function and Wnt signal modulation. *Curr. Top. Dev. Biol.* **85**, 175-195.

Gerlitz, G., Darhin, E., Giorgio, G., Franco, B. and Reiner, O. (2005). Novel functional features of the Lis-H domain: role in protein dimerization, half-life and cellular localization. *Cell Cycle* **4**, 1632-1640.

Guindon, S. and Gascuel, O. (2003). A simple, fast, and accurate algorithm to estimate large phylogenies by maximum likelihood. *Syst. Biol.* **52**, 696-704.

Jekely, G. and Arendt, D. (2006). Evolution of intraflagellar transport from coated vesicles and autogenous origin of the eukaryotic cilium. *BioEssays* **28**, 191-198.

Kavaslar, G. N., Onengut, S., Derman, O., Kaya, A. and Tolun, A. (2000). The novel genetic disorder microhydranencephaly maps to chromosome 16p13.3-12.1. *Am. J. Hum. Genet.* **66**, 1705-1709.

Kilburn, C. L., Pearson, C. G., Romijn, E. P., Meehl, J. B., Giddings, T. H., Jr, Culver, B. P., Yates, J. R., 3rd and Winey, M. (2007). New Tetrahymena basal body protein components identify basal body domain structure. *J. Cell Biol.* **178**, 905-912.

Kim, J. C., Badano, J. L., Sibold, S., Esmail, M. A., Hill, J., Hoskins, B. E., Leitch, C. C., Venner, K., Ansley, S. J., Ross, A. J. et al. (2004a). The Bardet-Biedl protein BBS4 targets cargo to the pericentriolar region and is required for microtubule anchoring and cell cycle progression. *Nat. Genet.* **36**, 462-470.

Kim, M. H., Cooper, D. R., Oleksy, A., Devedjiev, Y., Derewenda, U., Reiner, O., Otlewski, J. and Derewenda, Z. S. (2004b). The structure of the N-terminal domain of the product of the lissencephaly gene Lis1 and its functional implications. *Structure* **12**, 987-998.

Kubo, A. and Tsukita, S. (2003). Non-membranous granular organelle consisting of PCM-1: subcellular distribution and cell-cycle-dependent assembly/disassembly. *J. Cell Sci.* **116**, 919-928.

Kubo, A., Sasaki, H., Yuba-Kubo, A., Tsukita, S. and Shiina, N. (1999). Centriolar satellites: molecular characterization, ATP-dependent movement toward centrioles and possible involvement in ciliogenesis. *J. Cell Biol.* **147**, 969-980.

Lechtreck, K. F., Delmotte, P., Robinson, M. L., Sanderson, M. J. and Witman, G. B. (2008). Mutations in Hydin impair ciliary motility in mice. *J. Cell Biol.* **180**, 633-643.

Loktev, A. V., Zhang, Q., Beck, J. S., Searby, C. C., Scheetz, T. E., Bazan, J. F., Slusarski, D. C., Sheffield, V. C., Jackson, P. K. and Nachury, M. V. (2008). A BBSome subunit links ciliogenesis, microtubule stability, and acetylation. *Dev. Cell* **15**, 854-865.

Marshall, W. F. (2008). Basal bodies platforms for building cilia. *Curr. Top. Dev. Biol.* **85**, 1-22.

Marshall, W. F. and Rosenbaum, J. L. (2001). Intraflagellar transport balances continuous turnover of outer doublet microtubules: implications for flagellar length control. *J. Cell Biol.* **155**, 405-414.

Marshall, W. F. and Nonaka, S. (2006). Cilia: tuning in to the cell's antenna. *Curr. Biol.* **16**, R604-R614.

Marshall, W. F., Qin, H., Rodrigo Brenni, M. and Rosenbaum, J. L. (2005). Flagellar length control system: testing a simple model based on intraflagellar transport and turnover. *Mol. Biol. Cell* **16**, 270-278.

Megraw, T. L., Kilaru, S., Turner, F. R. and Kaufman, T. C. (2002). The centrosome is a dynamic structure that ejects PCM flares. *J. Cell Sci.* **115**, 4707-4718.

Mikolajka, A., Yan, X., Popowicz, G. M., Smialowski, P., Nigg, E. A. and Holak, T. A. (2006). Structure of the N-terminal domain of the FOP (FGFR1OP) protein and implications for its dimerization and centrosomal localization. *J. Mol. Biol.* **359**, 863-875.

Nachury, M. V., Loktev, A. V., Zhang, Q., Westlake, C. J., Peranen, J., Merdes, A., Slusarski, D. C., Scheller, R. H., Bazan, J. F., Sheffield, V. C. et al. (2007). A core complex of BBS proteins cooperates with the GTPase Rab8 to promote ciliary membrane biogenesis. *Cell* **129**, 1201-1213.

Ou, G., Blacque, O. E., Snow, J. J., Leroux, M. R. and Scholey, J. M. (2005). Functional coordination of intraflagellar transport motors. *Nature* **436**, 583-587.

Park, T. J., Mitchell, B. J., Abitua, P. B., Kintner, C. and Wallingford, J. B. (2008). Dishevelled controls apical docking and planar polarization of basal bodies in ciliated epithelial cells. *Nat. Genet.* **40**, 871-879.

Pazour, G. J. and Bloodgood, R. A. (2008). Targeting proteins to the ciliary membrane. *Curr. Top. Dev. Biol.* **85**, 115-149.

Pedersen, L. B. and Rosenbaum, J. L. (2008). Intraflagellar transport (IFT) role in ciliary assembly, resorption and signalling. *Curr. Top. Dev. Biol.* **85**, 23-61.

Popovici, C., Zhang, B., Gregoire, M. J., Jonveaux, P., Lafage-Pochitaloff, M., Birnbaum, D. and Pebusque, M. J. (1999). The t(6;8)(q27;p11) translocation in a stem cell myeloproliferative disorder fuses a novel gene, FOP, to fibroblast growth factor receptor 1. *Blood* **93**, 1381-1389.

Romio, L., Fry, A. M., Winyard, P. J., Malcolm, S., Woolf, A. S. and Feather, S. A. (2004). OFD1 is a centrosomal/basal body protein expressed during mesenchymal-epithelial transition in human nephrogenesis. *J. Am. Soc. Nephrol.* **15**, 2556-2568.

Satir, P. and Christensen, S. T. (2007). Overview of structure and function of mammalian cilia. *Annu. Rev. Physiol.* **69**, 377-400.

Sawin, K. E., Lourenco, P. C. and Snaith, H. A. (2004). Microtubule nucleation at non-spindle pole body microtubule-organizing centers requires fission yeast centrosomin-related protein mod20p. *Curr. Biol.* **14**, 763-775.

Singla, V. and Reiter, J. F. (2006). The primary cilium as the cell's antenna: signaling at a sensory organelle. *Science* **313**, 629-633.

Srsen, V., Gnadt, N., Dammermann, A. and Merdes, A. (2006). Inhibition of centrosome protein assembly leads to p53-dependent exit from the cell cycle. *J. Cell Biol.* **174**, 625-630.

Tassin, A. M., Celati, C., Moudjou, M. and Bornens, M. (1998). Characterization of the human homologue of the yeast spc98p and its association with gamma-tubulin. *J. Cell Biol.* **141**, 689-701.

Town, T., Breunig, J. J., Sarkisian, M. R., Spilianakis, C., Ayoub, A. E., Liu, X., Ferrandino, A. F., Gallagher, A. R., Li, M. O., Rakic, P. et al. (2008). The stumpy gene is required for mammalian ciliogenesis. *Proc. Natl. Acad. Sci. USA* **105**, 2853-2858.

Wheatley, D. N., Wang, A. M. and Strugnell, G. E. (1996). Expression of primary cilia in mammalian cells. *Cell Biol. Int.* **20**, 73-81.

Wong, S. Y. and Reiter, J. F. (2008). The primary cilium at the crossroads of mammalian hedgehog signaling. *Curr. Top. Dev. Biol.* **85**, 225-260.